THE JOURNAL OF PHYSICAL CHEMISTRY C
A JOURNAL OF THE AMERICAN CHEMICAL SOCIETY

pubs.acs.org/JPCC

Article

Odd–Even Effect in Electron Beam Irradiation of Hybrid Aromatic–Aliphatic Self-Assembled Monolayers of Fatty Acid

Monika Kruk, Christof Neumann, Martha Frey, Krzysztof Kozieł, Andrey Turchanin,* and Piotr Cyganik*

Cite This: *J. Phys. Chem. C* 2021, 125, 9310–9318

Read Online

ACCESS | Metrics & More | Article Recommendations | Supporting Information

ABSTRACT: Electron irradiation of aromatic self-assembled monolayers (SAMs) in combination with different lithographic approaches provides an interesting alternative for high-resolution surface patterning. More recently, it has been also demonstrated that this process can be used for carbon nanomembrane (CNM) fabrication, which forms technologically attractive 2D materials, with potential applications in different areas of nanotechnology such as ultrafiltration and nanobiosensing. To better understand the relation between the original SAM structure and the resulting CNM formation, in the current study, we conduct systematic analysis of the electron irradiation process for a model SAM system deposited on Ag substrates and based on a homologue series of biphenyl substituted carboxylic acids [$C_6H_5–C_6H_4–(CH_2)_n–COO/Ag$, $n = 2–6$] with different lengths of the aliphatic linker defined by the number n. Our results of X-ray photoelectron spectroscopy of irradiated monolayers show that the process of electron-induced desorption, cross-linking, and elimination of the SAM binding group depend on the parity of the parameter n (the odd–even effect). Our observations indicate a way for controlling thickness and purity of such nanomembranes, which are the key parameters determining the range of CNM applications.

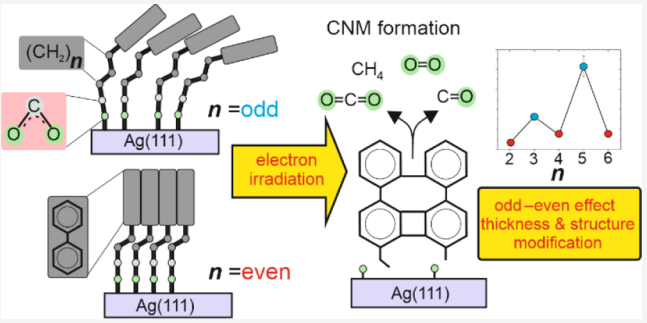

1. INTRODUCTION

The increased miniaturization of integrated devices used in organic and molecular electronics as well as in biology and medicine demands novel methods for surface and thin-film control at the microscale and nanoscale. Self-assembled monolayers (SAMs)[1,2] provide a simple way for functionalization of solid substrates by well-defined organic monolayers which become particularly attractive in combination with a variety of patterning methods[3] applied for building organic electronic devices[4] and controlling biocompatible interfaces.[5] In particular, electron-beam irradiation provides an effective means for SAM modification from the micrometer scale down to the nanometer scale. Depending on the chemical and structural composition of the monolayer, the interaction of electron beams with SAMs can be used to initiate different processes that include partial desorption,[6−8] cross-linking of aromatic molecules,[9−12] and surface modification of their chemical functionality.[13] As demonstrated in recent years, these fundamental processes in turn can be used for different types of lithography of organic[13−17] and inorganic[18,19] materials, the formation of chemical gradients on the surface,[20] metal substrate work function modification,[21] and transforming SAMs into carbon-based materials such as graphene[22,23] or carbon nanomembranes (CNMs).[24−27]

To date electron-beam irradiation experiments on SAMs were done almost exclusively using different types of thiols chemisorbed on the gold substrate. One of the exceptions are very recent experiments for hybrid aromatic–aliphatic[28] and purely aromatic[29,30] SAMs based on using carboxylic acid as an anchoring group to the silver substrate. It has been demonstrated that these SAMs can be successfully used for CNM formation of similar quality as in the case of analogous SAMs based on thiols.[28,29] Importantly, experiments performed for hybrid aromatic–aliphatic SAMs based on the biphenyl unit indicate that in contrast to SAMs based on thiols, the combination of desorption and the cross-linking process leads to elimination of the anchoring group and thus to the formation of free-standing CNMs without the chemically active group which is important for applications such as ultrafiltration.[28] This effect has not been reported for the purely aromatic carboxylic SAMs based on biphenyl[30] or terphenyl,[29] which indicates the crucial role of the aliphatic

Received: March 4, 2021
Revised: April 5, 2021
Published: April 21, 2021

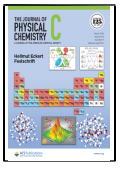

Downloaded via UNIWERSYTETU JAGIELLONSKIEGO on August 11, 2021 at 11:44:08 (UTC).
See https://pubs.acs.org/sharingguidelines for options on how to legitimately share published articles.

ACS Publications

© 2021 The Authors. Published by American Chemical Society

https://doi.org/10.1021/acs.jpcc.1c01857
J. Phys. Chem. C 2021, 125, 9310–9318

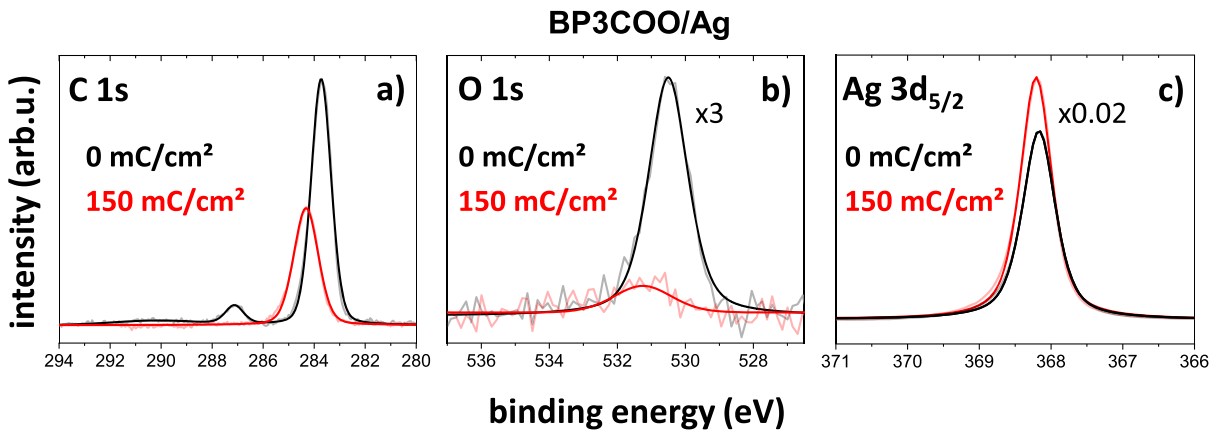

Figure 1. C 1s, O 1s, and Ag 3d XPS spectra for native and electron-beam-irradiated (a–c) BP3COO/Ag samples using an electron energy of 50 eV and a total electron dose of 150 mC/cm^2. The black and red lines mark signals for native and irradiated samples, respectively. For better presentation, intensities of the O 1s and Ag 3d$_{5/2}$ spectra are multiplied by the factor presented in the figure.

linker in the process of head group elimination. To elucidate the role of the aliphatic spacer on electron-induced modification of hybrid aromatic–aliphatic SAMs with the carboxylic head group, we analyze in the current study a series of $C_6H_5-C_6H_4-(CH_2)_n-COO/Ag$ (denoted as BP*n*COO/Ag, n = 2–6) SAMs. The structure formed by this homologue series was investigated in detail in former studies, which revealed that depending on the odd or even value of the parameter n, the BP*n*COO/Ag monolayers can form either a crystalline (n = even) or 2D disordered, liquid-like (n = odd) structure.[31] It was shown that the crystalline form of even members of the BP*n*COO/Ag series is associated with the more upright orientation of the biphenyl unit and the anchoring carboxylic group, both of which result in a higher packing density of molecules on the Ag(111) surface and a higher thickness of the monolayer.[31] Consequently, for the liquid-like structure of odd members, the lower packing density and film thickness are the results of the more canted orientation of both the biphenyl unit and the anchoring group.[31] The observed structural odd–even effect was explained by the simple, qualitative model in which for even members of the series, the three main contributions to the overall energetics of the system such as packing density (density of the COO–Ag bonds), the Ag–O–C bending potential, and the intermolecular interactions act in a cooperative way, that is, they are satisfied by the same configuration of molecules and thus lead to a well-defined and stable monolayer. In contrast, for odd members of the series, the more canted orientation of the biphenyl group leads to the reduction in packing density and intermolecular interactions, both of which can be improved only at the price of changing the Ag–O–C bending potential from its optimal configuration. As a result, the competitive relationship between these three factors results in the 2D disordered liquid-like structure and lower stability of odd-numbered BP*n*COO/Ag SAMs. Thus, this strong structural odd–even effect gives us a unique opportunity to test if the modification of the adsorption geometry (the molecular backbone and adsorption group), packing density, and the type of 2D ordering (crystalline vs liquid-like structure) of SAMs can influence their modification by the electron beam and, as a result of this process, the formation of the CNMs. We note at this point that our analysis has much broader context since the odd–even structural effects in SAMs[32] have also been reported for other hybrid aliphatic–aromatic monolayers based on thiols[33−41] and selenols[42−44] on Au or Ag substrates with some of studies devoted to their impact on the electron[45] or ion[46] beam-induced modification of SAMs.

2. EXPERIMENTAL METHODS

2.1. SAM Preparation. The $C_6H_5-C_6H_4-(CH_2)_n-COO$ (BP*n*COOH) compounds with n = 2 and n = 3–4 were purchased from Alfa Aesar and Wako, respectively. The synthesis procedure of BP*n*COOH compounds with n = 5–6 is described elsewhere.[47] The Ag(111) substrates were prepared by evaporation of ∼100 nm (rate 0.1 nm/s) of silver on mica sheets at 533 K. All SAMs were prepared by immersion (5 min) of Ag(111) substrates in the solution (1 mM) of the respective compound in absolute ethanol (99.8%, POCH-Poland). After incubation, the samples were rinsed with pure ethanol and dried under a nitrogen stream.

2.2. Electron Irradiation. The electron irradiation was performed in the same ultra-high-vacuum (UHV) system as used for the X-ray photoelectron spectroscopy (XPS) analysis with a 50 eV electron beam generated using an NEK-SC 150 (Staib) electron gun.

2.3. X-ray Photoelectron Spectroscopy. XPS was performed *in situ* using a Multiprobe system (Scienta Omicron) in UHV (base pressure 2 × 10^{-10} mbar) equipped with a monochromatic X-ray source (Al K$_\alpha$) and an electron analyzer (Argus CU) with a 0.6 eV spectral energy resolution. The binding energy (BE) scale was calibrated using the Ag 3d$_{5/2}$ peak as a reference (BE = 368.2 eV).[48] All spectra were fitted by Voigt functions (30:70) after background subtraction using the linear (O 1s) or Shirley (C 1s, Ag 3d) function.

3. RESULTS AND DISCUSSION

The process of electron irradiation was monitored *in situ* using XPS with respective data and analysis summarized in Figures 1–5. To indicate the main features of the XPS spectra, the data obtained for the BP3COO/Ag sample are presented in Figure 1 as a representative example for the entire homologue series of BP*n*COO/Ag (n = 2–6) SAMs. The C 1s spectrum for native BP3COO/Ag (Figure 1a, black) shows the main peak located at a BE of ∼283.7 eV, which is due to the biphenyl moiety and the short aliphatic spacer. It also reveals a smaller component at BE ∼ 287.1 eV due to the COO– group involved in the bidentate Ag–carboxylate bond.[28,31,49] This

https://doi.org/10.1021/acs.jpcc.1c01857
J. Phys. Chem. C 2021, 125, 9310−9318

assignment is more directly confirmed by the O 1s spectrum shown in Figure 1b, which can be described by a single peak located at BE ∼ 530.4 eV.[28,31,49] The general effect of low-energy electron irradiation of BP3COO/Ag is exemplified in Figure 1a−c. As shown in Figure 1a for the main C 1s component, associated with the biphenyl and aliphatic part of the backbone, the increased dose of electron irradiation leads to gradual reduction in the intensity together with the pronounced shift toward higher values of BE. In contrast, the high-energy C 1s component, associated with the carboxylic group, vanishes for high electron doses. This behavior is fully correlated with the O 1s spectra which for high electron doses exhibit almost complete signal loss (Figure 1b), confirming electron-induced removal of the carboxylic bonding group. The drop of the C 1s and O 1s signals is also consistent with the electron irradiation-induced increase of the Ag $3d_{5/2}$ signal intensity as a result of the monolayer thickness reduction (Figure 1c). We note that apart from the increase in the Ag $3d_{5/2}$ signal intensity, the electron irradiation of BP*n*COO/Ag also resulted in certain reduction of the peak full width at half-maximum (fwhm) by ∼50 meV and the shift of the BE toward higher values by ∼40 meV. Considering former synchrotron-based high-resolution XPS studies comparing the Ag $3d_{5/2}$ signal for the bar Ag(111) substrate and after adsorption of SAMs,[50] these observations are consistent with the modification of the surface component of the Ag $3d_{5/2}$ signal due to the electron-induced elimination of the chemical bonding of BP*n*COO molecules with the Ag substrate and partial desorption of the monolayer.

To discuss the electron-beam-induced modification of the BP*n*COO/Ag SAMs in more detail, we analyze first the intensity of the C 1s signal. As shown in Figure 1, the electron irradiation of BP*n*COO/Ag SAMs leads to a significant drop of the carbon signal. This drop is associated with the partial desorption of the monolayer and reduction of the effective film thickness (d) which can be calculated using a standard procedure based on the C 1s/Ag 3d intensity ratios,[8,51] assuming exponential attenuation of the photoelectron signal with attenuation lengths ($\lambda_{Ag3d5/2}$ = 26.8 Å and λ_{C1s} = 28.08 Å) calculated on the basis of previously reported analysis[52] and taking as a reference the film thickness of HDT/Ag (HDT—hexadecane thiol) SAMs measured in the same experiment. The effect of film thickness reduction as a function of the electron irradiation dose is presented in Figure 2a using BP3COO/Ag as a representative example (see Figure S1 in the Supporting Information file for the complete set of data). To calculate the characteristic thickness cross-section (σ_{TH}) for this process, we have used the standard saturation function[7,53] defined as

$$d(Q/S) = d_{SAT} + (d_0 - d_{SAT})\cdot\exp\left(\frac{-\sigma_{TH}\cdot Q}{e\cdot S}\right) \quad (1)$$

where d_0 and d_{SAT} are the thicknesses for the native and extensively irradiated monolayers, respectively, and Q/S [C/m^2] is the primary electron irradiation dose. The values of the d_0 and d_{SAT} parameters obtained for the BP*n*COO/Ag series are presented in Figure 2b. In agreement with former structural analysis,[31] the increase of the thickness d_0 of the native monolayer with the parameter n is overlaid with an additional odd−even modulation as a consequence of the odd−even variation in the tilt of both the biphenyl moiety and the carboxylate bonding group toward the silver substrate. The

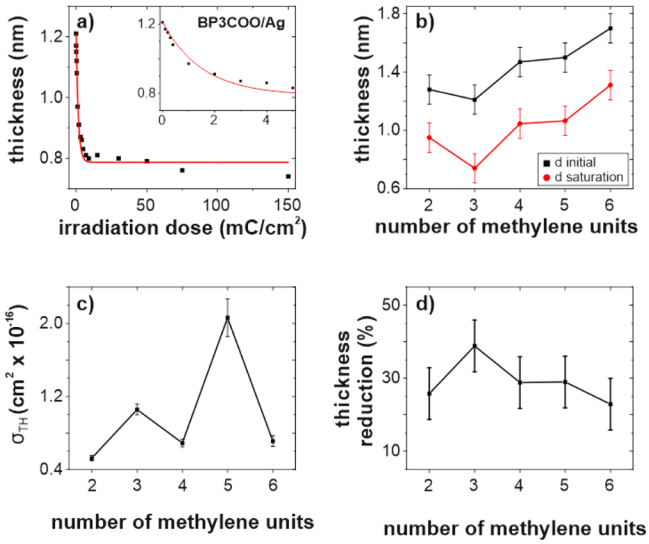

Figure 2. Electron-induced modification (electron energy 50 eV) of film thickness for BP*n*COO/Ag (n = 2−6). (a) Film thickness as a function of the electron irradiation dose for the BP3COO/Ag sample. (b) Film thickness before and after (saturation level) electron irradiation. (c) Cross-section for this process. (d) Thickness reduction as a function of the parameter n.

extensive electron irradiation process leads to reduction of the initial monolayer thickness d_0 to the value defined by d_{SAT}. As evident from the data presented in Figure 2b, the parameter d_{SAT} exhibits similar dependence to d_0, that is, a general growth with the parameter n with an additional odd−even variation, which has the same phase as for the native monolayer. The calculated values of the respective cross-sections σ_{TH} are presented in Figure 2c and show pronounced odd−even dependence with significantly higher values obtained for odd-numbered members of the BP*n*COO/Ag series. As shown in Figure 2d, the odd−even variation of σ_{TH} is also correlated with the odd−even variation of the percentage of the total thickness reduction defined as $(d_0 - d_{SAT})/d_0 \times 100\%$. A higher efficiency of the thickness reduction process (higher σ_{TH}) observed for odd-numbered monolayers indicates a more effective electron-induced desorption process which has to be correlated with their structural difference compared to even-numbered monolayers. As pointed above, former spectroscopic and microscopic analysis[31] revealed that odd-numbered BP*n*COO/Ag SAMs exhibit a lower packing density and a disordered, liquid-like structure, which are associated with a more canted orientation of biphenyl and anchoring groups. These structural features of odd-numbered monolayers indicate lower intermolecular interactions compared to highly ordered, and densely packed, even-numbered monolayers, which can increase the efficiency of the desorption process of molecules, and their fragments, after electron-induced cleavage of a given chemical bond. The higher percentage of the total thickness reduction for odd-numbered monolayers indicates that the cross-linking process, which hampers further electron-induced desorption of the aromatic monolayer, is less effective in this case, and thus, the desorption process is continued longer during the initial steps of electron irradiation. Since the cross-linking process is mainly related to the electron-induced C−H bond scission and the subsequent formation of new C−C bonds between biphenyl units of neighboring molecules in the monolayer, the lower packing density and the disordered

https://doi.org/10.1021/acs.jpcc.1c01857
J. Phys. Chem. C 2021, 125, 9310−9318

structure of these units for odd-numbered BP*n*COO/Ag may explain the lower efficiency of this process in this case. The range of σ_{TH} values for thickness reduction reported here ($\sigma_{TH} \sim (0.5 - 2.0) \times 10^{-16}$ cm^2) for BP*n*COO/Ag is lower compared to recently published analogous analysis[8] obtained for 50 eV electron irradiation of SAMs based on alkanethiols ($\sigma_{TH} \sim (3 - 4) \times 10^{-16}$ cm^2). Such a difference confirms the much higher efficiency of the cross-linking process in the case of BP*n*COO/Ag systems which effectively quenches desorption and thus thickness reduction upon electron irradiation. The same mechanism was also reported earlier for purely aromatic SAMs based on biphenyl thiols and selenols where even lower values of cross-section for thickness reduction were reported ($\sim 2 \times 10^{-17}$ cm^2).[54] In fact, we expect that the efficiency of the cross-linking process for BP*n*COO/Ag compared to that for alkanethiols must be even higher considering very efficient elimination of the anchoring group in the case of BP*n*COO/Ag (*vide infra*) with at the same time very little efficiency of this process for SAMs based on thiols on the Ag[25] or Au[8,55] substrate.

As shown in Figure 1a, together with the intensity, the position, that is, the BE of the main component of C 1s, is modified upon electron irradiation. A detailed analysis of this effect is shown in Figure 3a for BP3COO/Ag as a function of

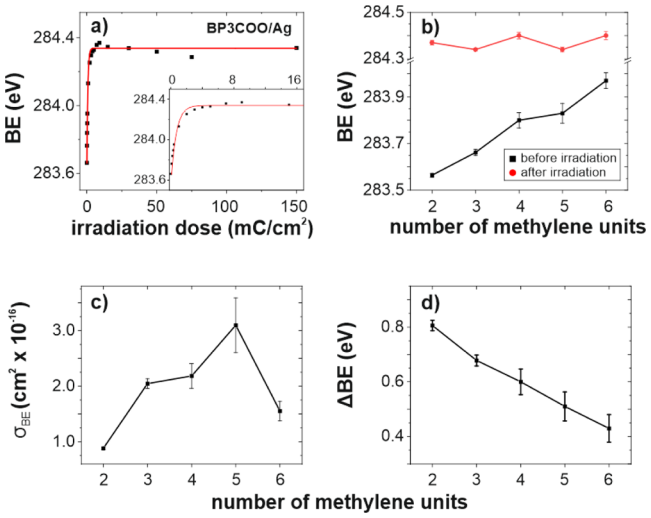

Figure 3. Electron-induced BE modification (electron energy 50 eV) of the main C 1s XPS peak for BP*n*COO/Ag (n = 2–6). (a) BE as a function of the electron irradiation dose (energy 50 eV) for the BP3COO/Ag sample. (b) BE before and after electron irradiation (energy 50 eV, dose 150 mC/cm^2) as a function of the parameter n, (c) cross-section for this process as a function of the parameter n, and (d) change in BE due to electron irradiation as a function of the number n.

the electron dose (see Figure S2 in the Supporting Information file for the complete set of data). Obtained data exhibit gradual transition of BE from the value characteristic for the native monolayer toward a much higher value of BE which saturates at high irradiation doses and can be described by the analogous saturation function as defined by eq 1. While such behavior is common for all members of the BP*n*COO/Ag (n = 2–6) series, the data presented in Figure 3b show that the value of the BE for the native, and to some extent also for fully electron-beam-modified samples (i.e., at the dose of 150 mC/cm^2), depends on the parameter n. In particular, for the native samples, the respective BE value gradually grows with the increased value of n from ~283.5 eV for n = 2 up to ~284.0 eV for n = 6. To explain this effect as a first point, we note that previous analysis comparing full analogue BP2S/Ag and BP2COO/Ag monolayers[28,49] revealed for the former system significantly higher values of the BE for the C 1s main component in the range of ~284.2–284.5 eV. A similar range of BEs was also recently reported for a variety of aromatic SAMs based on thiols on Au with the oligophenyl, acene, or oligo(phenylene ethynylene) backbone.[55] This shift in the BE for the C 1s main component toward a lower energy (by ~0.8–0.5 eV) associated with the modification of the bonding group from thiolate to carboxylate can be attributed to the charge rearrangement at the molecule–metal interface[56] which for the COO– based SAMs leads to the formation of an interfacial dipole layer oriented toward the metal surface and most probably originating from the ionic O–Ag bond formation. The normal (perpendicular to the metal surface) component of such a dipole layer lowers the BE of the C 1s level for all carbon atoms located above the dipole layer. Since this effect should decrease with the increased vertical distance of a given carbon atom from the dipole layer, we expect that the resulting shift in the C 1s BE, which is measured as an averaged value over all carbon atoms belonging to the biphenyl moiety and the aliphatic spacer, should be reduced for longer molecules, as indeed observed for the BP*n*COO/Ag series in Figure 3b. Moreover, considering that the odd–even modification of the parameter n in BP*n*COO/Ag induces reorientation of the biphenyl moiety which is more tilted toward the Ag surface for odd-numbered monolayers,[31] one could expect a lower BE of the C 1s spectra for odd-numbered members of the series (due to a smaller average distance from the surface dipole layer). This additional effect, although much weaker, is overlaid on the length dependence visible in Figure 3b. We note at this point that the odd–even variation of the C 1s BE was also reported[33] earlier for BP*n*S/Ag SAMs (n = 3–6) with higher BE values for even-numbered members of the series, similar to the current analysis for BP*n*COO/Ag series. Considering the same phase of the structural odd–even effect in both systems[31,33,34] as well as the same orientation of the normal component of the surface dipole moment (toward the metal surface) for S–Ag[57,58] and O–Ag[28,31,49] bonds associated with the charge transfer to the anchoring group, this effect is consistent with currently proposed explanation.

The BE of the main C 1s signal for electron-irradiated BP*n*COO/Ag SAMs reached a saturation value of ~284.4 eV, which is also close to the values reported earlier for other electron-irradiated aromatic SAMs based on thiols[28,45,55] (see Figure 3b). In former studies analyzing electron irradiation of aromatic SAMs,[55] the change in BE toward a higher energy was attributed to chemical modification of the film structure via electron-induced scission of the C–H bonds and the subsequent cross-linking process. However, the electron irradiation-induced change of the BE reported here (Figure 3d) for BP*n*COO/Ag SAMs is ~5–8 times bigger as compared to those reported earlier for thiol-based aromatic SAMs on the Au surface despite the same mechanism of the cross-linking process.[55] Therefore, current results indicate that at least for BP*n*COO/Ag SAMs, the pronounced modification of the C 1s BE can be primary attributed to the electron irradiation-induced destruction of the molecule–substrate dipole layer via termination of the Ag–O bonding formed in the case of BP*n*COO/Ag SAMs as confirmed by the shift in BE for native

https://doi.org/10.1021/acs.jpcc.1c01857
J. Phys. Chem. C 2021, 125, 9310–9318

monolayers with carboxylate and thiolate anchoring groups and much more effective elimination of the bonding group for these SAMs during electron irradiation (*vide infra*). Following such interpretation, a weak odd−even variation of the BE saturation level visible in Figure 3b, with slightly higher values for even-numbered members of the series, indicates that the level of the molecule−substrate dipole layer elimination and/or the film thickness of the electron-irradiated monolayer is higher in this case. Since the level of oxygen concentration upon complete electron irradiation (*vide infra*) shows an appositive odd−even relation (Figure 4b), we attribute this effect to the film thickness measured upon electron irradiation which shows the same phase of the odd−even relation (Figure 2b).

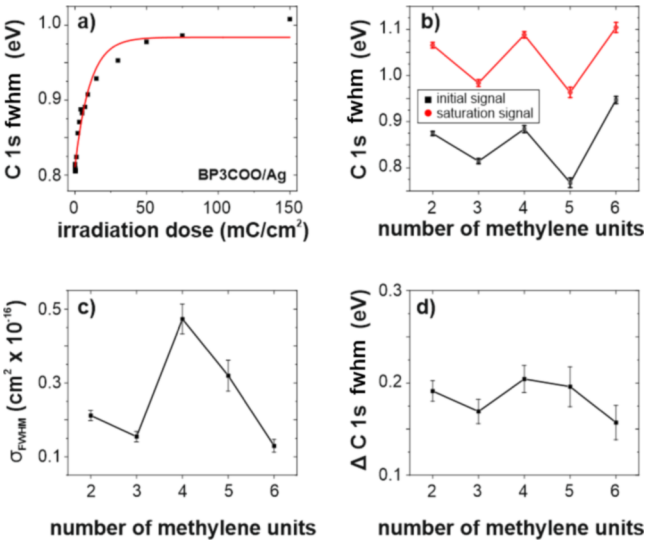

Figure 4. Electron-induced (electron energy 50 eV) fwhm modification of the main C 1s XPS peak for BP*n*COO/Ag (n = 2−6). (a) C 1s fwhm as a function of the electron irradiation dose for BP3COO/Ag (electron energy 50 eV). (b) C 1s fwhm before and after (saturation level) electron irradiation as a function of the parameter n, (c) cross-section for this process as a function of the parameter n, and (d) change in fwhm due to electron irradiation as a function of the parameter n.

The values of the cross-section related to BE modification (σ_{BE}) are presented in Figure 3c and show odd−even variation with higher values calculated for odd-numbered members of the series. The phase of this odd−even effect is the same as that for σ_{TH}, thus indicating correlation of the O−Ag bond termination and reduction in film thickness.

The final point of the C 1s signal analysis was the fwhm. As shown in Figure 4a for BP3COO/Ag, the electron irradiation leads to an increase of this parameter which follows the saturation function (see Figure S3 in the Supporting Information file for the complete set of data). The data presented in Figure 4b show that this effect is common for all members of the BP*n*COO/Ag series analyzed here. A similar increase in fwhm was also reported in former analysis of electron irradiation of both aliphatic[8] and aromatic[55,59] SAMs. The analysis conducted in the current study additionally reveals the odd−even effect related to the fwhm parameter with higher values for even-numbered members of the BP*n*COO/Ag series observed for native and fully electron-irradiated samples (Figure 4b). The respective cross-section (σ_{FWHM}) calculated for this process also reveals odd−even behavior with exception of data obtained for the BP6COO/Ag sample which does not fit to such a trend (Figure 4c).

A similar level of increase in the fwhm of C 1s upon electron irradiation[55,59] as well as a similar value of the respective cross-sections (σ_{FWHM}) calculated in the current study and reported in former analysis for aromatic SAMs[55] appears quite intuitive and related to a common cross-linking process which by the formation of new C−C/C═C bonds and elimination of the C−H bonds increases chemical inhomogeneity of the monolayer and thus broadening of the C 1s peak. However, the same phase and similar amplitude of the odd−even effect in fwhm observed for the native and irradiated BP*n*COO/Ag series are more difficult to explain. Considering, however, a former study[55,59] comparing few different types of aromatic SAMs with levels of differences in fwhm values measured for native and irradiated samples similar to those reported here[40,47] as well as those in the calculated cross-sections,[55] we suppose that observed odd−even effects in the fwhm parameter are related to odd−even structural differences in packing density and orientation of molecules which are, apparently, partially preserved upon irradiation.

In the final step of our analysis, we have monitored the relative change in oxygen concentration in the monolayer as a function of the electron irradiation dose. To estimate this parameter, we did not directly use the intensity of the measured O 1s signal (I_{mO1s}) but the corrected intensity (I_{cO1s}), which is proportional to the oxygen concentration considering exponential decay of the O 1s signal during transmission through the monolayer of a given film thickness in the form

$$I_{cO1s} = I_{mO1s} \cdot \exp\left(\frac{d}{\lambda_{O1s}}\right) \quad (2)$$

where λ_{O1s} = 24.25 Å is the attenuation length for electrons emitted from the O 1s level calculated according to the data in ref 52 and d is the film thickness for the given irradiation dose as presented in Figure 2b. Based on this calculation, the normalized value of the oxygen concentration as a function of the irradiation dose is presented in Figure 5a for BP3COO/Ag as a representative example (see Figure S4 in the Supporting Information file for the complete set of data). Similar to the film thickness, the drop of oxygen concentration, monitored by the I_{cO1s} signal, exhibits behavior which can be described by the saturation function defined by eq 1. The values of this signal obtained for the native film and at the saturation level of the irradiation process are presented in Figure 5b for the entire BP*n*COO/Ag series. The native concentration of oxygen (measured in arbitrary units) reveals a pronounced odd−even effect with a higher concentration for even-numbered members of the series in agreement with former analysis[31] indicating a higher packing density for these types of monolayers. This native odd−even relation is also partially preserved at the saturation point of the electron irradiation. The cross-section for oxygen elimination (σ_O) also exhibits a well-defined odd−even effect with higher values for odd-numbered members of the series (Figure 5c). This odd−even effect has the same phase as the odd−even effects observed in the cross-sections for BE (σ_{BE}) and film thickness (σ_{TH}) modification. The correlation of the odd−even effect in the efficiency of BE modification (σ_{BE}) with the odd−even effect in the efficiency of oxygen elimination (σ_{BE}) confirms the above proposed

https://doi.org/10.1021/acs.jpcc.1c01857
J. Phys. Chem. C 2021, 125, 9310−9318

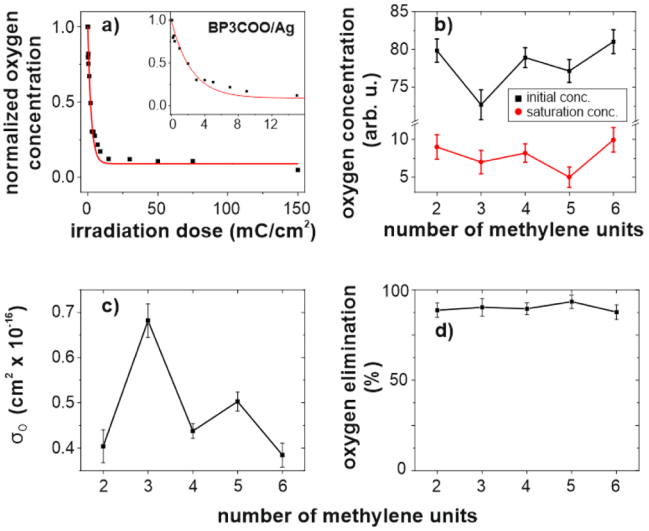

Figure 5. Electron-induced modification (electron energy 50 eV) of the oxygen concentration for BP*n*COO/Ag (n = 2−6) based on XPS data. (a) Normalized oxygen concentration as a function of the electron irradiation dose for BP3COO/Ag. (b) Oxygen concentration before and after (saturation level) electron irradiation as a function of the parameter n, (c) cross-section for this process as a function of the parameter n, and (d) oxygen reduction as a function of the number n.

model in which the shift in BE of the C 1s level is associated with the electron-induced destruction of the dipole layer formed at the molecule−metal interface by the polarized O−Ag bonds.

The correlation of odd−even effects for σ_{TH} and σ_O is more complicate to analyze. First, we note that while the elimination of oxygen during the electron irradiation process analyzed here is almost complete (Figure 5d), the reduction of the corresponding film thickness is on the level of only ∼30% (Figure 2d). This indicates that despite the fact that oxygen is responsible for chemical bonding of individual molecules with the metal substrate, its elimination is still possible without complete desorption of the monolayer. This is a result of the electron-induced cross-linking process which stabilizes the monolayer during oxygen elimination. The elimination of oxygen has two separate stages. The first stage is termination of the respective chemical bonds, that is, Ag−O and O−C, and the second is the desorption process of oxygen or oxygen-containing molecular fragments. Both stages have different controlling factors. The process of bond termination via electron irradiation is controlled by the efficiency of the electron-induced excitation to the dissociative state and by the possible relaxation process from this state which prevents bond termination. The electron-induced excitation will depend on the flux of electrons at the point of excitation. We note that to reach the carboxylic bonding group located at the metal interface, the electron beam has to pass through the monolayer. Considering an attenuation length of ∼6.5 Å for 50 eV electrons during their transmission through SAMs,[52] this flux can be increased by ∼36% by reducing the SAM thickness by just 2 Å. Therefore, the reduced thickness for the odd-numbered BP*n*COO/Ag SAMs can amplify the efficiency of Ag−O and O−C bond termination, thus correlating the odd−even effects in cross-sections of film thickness (σ_{TH}) and oxygen elimination (σ_O). Moreover, when excitation of a given bond is located in the molecule chemisorbed to the metal surface, as is the case for the metal bonding carboxylic group in BP*n*COO/Ag SAMs, the efficiency of bond termination is strongly controlled by the non-radiative decay process which involves charge transfer between the excited state and the metal substrate.[60] Thus, the efficiency of the electron-induced bond termination in SAMs for chemical bonds located close to the metal surface critically depends on the local electronic structure at the molecule−metal interface.[53,60] Considering that the odd−even structural effect in BP*n*COO/Ag SAMs leads to an odd−even modification of the carboxylate bonding group conformation, as is evident from former infrared reflection absorption spectroscopy analysis,[31] we can suppose that this will result in an odd−even efficiency of the electron-induced C−O or Ag−O bond termination. The magnitude and the phase of this odd−even effect remain unknown at the moment considering the unknown impact of the carboxylate bonding conformation on the charge-transfer process. As pointed above, the desorption of oxygen, and oxygen-containing molecular fragments, is a separate process which is controlled by the efficiency of intermolecular interactions, steric limitations, and the thickness of the film through which these species have to be transmitted. These parameters in turn depend on monolayer packing density, the efficiency of the cross-linking process during film irradiation, and the resulting film thickness. The film thickness modification is controlled by the desorption of molecules and the cross-linking process which hampers desorption. The data in Figure 2 indicate that for odd-numbered members of the BP*n*COO/Ag series, thickness modification is more pronounced with a lower efficiency of the cross-linking process. Higher desorption of molecules, a lower packing density, a less efficient cross-linking process, and the lower value of the cross-linked film thickness are all consistent with more pronounced elimination of oxygen. Summarizing this part, we come to the conclusion that all main physical processes involved in electron-beam-induced oxygen elimination indicate high sensitivity to the odd−even structural modification of BP*n*COO/Ag SAMs. Moreover, in the case of the initial electron excitation efficiency as well as the final desorption probability, the correlation of the odd−even behavior for σ_O and σ_{TH} is well justified.

4. SUMMARY AND CONCLUSIONS

Detailed XPS analysis of an electron-beam-irradiated homologue series of hybrid aliphatic−aromatic SAMs of BP*n*COO/Ag presented here revealed a significant role of the aliphatic spacer (defined by the parameter n) in the electron-induced desorption/modification of such monolayers and as a result the structure and purity of the CNMs produced by this process as well. Our data show that partial desorption of the monolayer upon electron irradiation, and thus the resulting effective thickness of the CNMs, is more efficient for odd-numbered members of the series. This odd−even effect is correlated with the odd−even differences in the structure of BP*n*COO/Ag which for odd-numbered members of the series have a disordered liquid-like structure with a lower packing density and thus less effective molecule−molecule interactions controlling the efficiency of the desorption process upon electron-beam-induced termination of the chemical bonding with the substrate. We show that electron irradiation also leads to almost complete elimination of oxygen from the system, which is confirmed not only directly by the concentration of this element in the monolayer but also indirectly by destruction of the interfacial dipole layer which is formed by the O−Ag bonds. The process of oxygen elimination also

https://doi.org/10.1021/acs.jpcc.1c01857
J. Phys. Chem. C 2021, 125, 9310−9318

shows the odd−even dependence with a higher efficiency for odd-numbered members of the series, that is, it is also correlated with the structural odd−even effect, similar to the case of the thickness reduction process.

■ ASSOCIATED CONTENT

Supporting Information

The Supporting Information is available free of charge at https://pubs.acs.org/doi/10.1021/acs.jpcc.1c01857.

Electron irradiation data obtained for BP*n*COO/Ag SAMs (with n = 2, 4, 5, 6) (PDF)

■ AUTHOR INFORMATION

Corresponding Authors

Andrey Turchanin − *Institute of Physical Chemistry, Friedrich Schiller University Jena, Jena 07743, Germany;* orcid.org/0000-0003-2388-1042; Email: andrey.turchanin@uni-jena.de

Piotr Cyganik − *Smoluchowski Institute of Physics, Jagiellonian University, Krakow 30-348, Poland;* orcid.org/0000-0001-6131-4618; Email: piotr.cyganik@uj.edu.pl

Authors

Monika Kruk − *Smoluchowski Institute of Physics, Jagiellonian University, Krakow 30-348, Poland*

Christof Neumann − *Institute of Physical Chemistry, Friedrich Schiller University Jena, Jena 07743, Germany*

Martha Frey − *Institute of Physical Chemistry, Friedrich Schiller University Jena, Jena 07743, Germany*

Krzysztof Kozieł − *Faculty of Chemistry, Jagiellonian University, Krakow 30-387, Poland;* orcid.org/0000-0002-3376-0861

Complete contact information is available at: https://pubs.acs.org/10.1021/acs.jpcc.1c01857

Notes

The authors declare no competing financial interest.

■ ACKNOWLEDGMENTS

C.N. and A.T. thank the Deutsche Forschungsgemeinschaft (DFG, German Research Foundation) for support within the research grants TU149/8−2 and 364549901—TRR 234 "CataLight" (B7, Z2) and the research infrastructure grant INST 275/25 7−1 FUGG. P.C. thanks Priority Research Area SciMat under the program Excellence Initiative—Research University at the Jagiellonian University in Kraków. This work was supported financially by the National Science Centre, Poland (grant UMO-2015/19/B/ST5/01636).

■ REFERENCES

(1) Love, J. C.; Estroff, L. A.; Kriebel, J. K.; Nuzzo, R. G.; Whitesides, G. M. Self-Assembled Monolayers of Thiolates on Metals as a Form of Nanotechnology. *Chem. Rev.* **2005**, *105*, 1103−1170.

(2) Gooding, J. J.; Ciampi, S. The Molecular Level Modification of Surfaces: From Self-Assembled Monolayers to Complex Molecular Assemblies. *Chem. Soc. Rev.* **2011**, *40*, 2704−2718.

(3) Smith, R. K.; Lewis, P. A.; Weiss, P. S. Patterning Self-Assembled Monolayers. *Prog. Surf. Sci.* **2004**, *75*, 1−68.

(4) Schmaltz, T.; Sforazzini, G.; Reichert, T.; Frauenrath, H. Self-Assembled Monolayers as Patterning Tool for Organic Electronic Devices. *Adv. Mater.* **2017**, *29*, 1605286.

(5) Clegg, J. R.; Wagner, A. M.; Shin, S. R.; Hassan, S.; Khademhosseini, A.; Peppas, N. A. Modular Fabrication of Intelligent Material-Tissue Interfaces for Bioinspired and Biomimetic Devices. *Prog. Mater. Sci.* **2019**, *106*, 100589.

(6) Müller, H. U.; Zharnikov, M.; Völkel, B.; Schertel, A.; Harder, P.; Grunze, M. Low-Energy Electron-Induced Damage in Hexadecanethiolate Monolayers. *J. Phys. Chem. B* **1998**, *102*, 7949−7959.

(7) Zharnikov, M.; Frey, S.; Heister, K.; Grunze, M. Modification of Alkanethiolate Monolayers by Low Energy Electron Irradiation: Dependence on the Substrate Material and on the Length and Isotopic Composition of the Alkyl Chains. *Langmuir* **2000**, *16*, 2697−2705.

(8) Schmid, M.; Wan, X.; Asyuda, A.; Zharnikov, M. Modification of Self-Assembled Monolayers by Electron Irradiation: The Effect of Primary Energy (10−500 eV). *J. Phys. Chem. C* **2019**, *123*, 28301−28309.

(9) Geyer, W.; Stadler, V.; Eck, W.; Zharnikov, M.; Gölzhäuser, A.; Grunze, M. Electron-Induced Crosslinking of Aromatic Self-Assembled Monolayers: Negative Resists for Nanolithography. *Appl. Phys. Lett.* **1999**, *75*, 2401−2403.

(10) Zharnikov, M.; Grunze, M. Modification of Thiol-Derived Self-Assembling Monolayers by Electron and X-Ray Irradiation: Scientific and Lithographic Aspects. *J. Vac. Sci. Technol., B: Microelectron. Nanometer Struct.–Process., Meas., Phenom.* **2002**, *20*, 1793−1807.

(11) Cyganik, P.; Vandeweert, E.; Postawa, Z.; Bastiaansen, J.; Vervaecke, F.; Lievens, P.; Silverans, R. E.; Winograd, N. Modification and Stability of Aromatic Self-Assembled Monolayers upon Irradiation with Energetic Particles. *J. Phys. Chem. B* **2005**, *109*, 5085−5094.

(12) Turchanin, A.; Käfer, D.; El-Desawy, M.; Wöll, C.; Witte, G.; Gölzhäuser, A. Molecular Mechanisms of Electron-Induced Cross-Linking in Aromatic SAMs. *Langmuir* **2009**, *25*, 7342−7352.

(13) Eck, W.; Stadler, V.; Geyer, W.; Zharnikov, M.; Gölzhäuser, A.; Grunze, M. Generation of Surface Amino Groups on Aromatic Self-Assembled Monolayers by Low Energy Electron Beams - A First Step Towards Chemical Lithography. *Adv. Mater.* **2000**, *12*, 805−808.

(14) Turchanin, A.; Schnietz, M.; El-Desawy, M.; Solak, H. H.; David, C.; Gölzhäuser, A. Fabrication of Molecular Nanotemplates in Self-Assembled Monolayers by Extreme-Ultraviolet-Induced Chemical Lithography. *Small* **2007**, *3*, 2114−2119.

(15) Turchanin, A.; Tinazli, A.; El-Desawy, M.; Großmann, H.; Schnietz, M.; Solak, H. H.; Tampé, R.; Gölzhäuser, A. Molecular Self-Assembly, Chemical Lithography, and Biochemical Tweezers: A Path for the Fabrication of Functional Nanometer-Scale Protein Arrays. *Adv. Mater.* **2008**, *20*, 471−477.

(16) Ballav, N.; Thomas, H.; Winkler, T.; Terfort, A.; Zharnikov, M. Making Protein Patterns by Writing in a Protein-Repelling Matrix. *Angew. Chem., Int. Ed.* **2009**, *48*, 5833−5836.

(17) Ballav, N.; Schlip, S.; Zharnikov, M. Electron Beam Chemical Lithography with Aliphatic Self-Assembled Monolayers. *Angew. Chem., Int. Ed.* **2008**, *47*, 1421−1424.

(18) Küller, A.; Eck, W.; Stadler, V.; Geyer, W.; Gölzhäuser, A. Nanostructuring of Silicon by Electron-Beam Lithography of Self-Assembled Hydroxybiphenyl Monolayers. *Appl. Phys. Lett.* **2003**, *82*, 3776−3778.

(19) Abufager, P. N.; Solano Canchaya, J. G.; Wang, Y.; Alcamí, M.; Martín, F.; Alvarez Soria, L.; Martiarena, M. L.; Reuter, K.; Busnengo, H. F. Theoretical Study of the Structure of Self-Assembled Monolayers of Short Alkylthiolates on Au(111) and Ag(111): The Role of Induced Substrate Reconstruction and Chain−Chain Interactions. *Phys. Chem. Chem. Phys.* **2011**, *13*, 9353−9362.

(20) Ballav, N.; Shaporenko, A.; Terfort, A.; Zharnikov, M. A Flexible Approach to the Fabrication of Chemical Gradients. *Adv. Mater.* **2007**, *19*, 998−1000.

(21) Sauter, E.; Yildirim, C.; Terfort, A.; Zharnikov, M. Adjustment of the Work Function of Pyridine and Pyrimidine Substituted Aromatic Self-Assembled Monolayers by Electron Irradiation. *J. Phys. Chem. C* **2017**, *121*, 12834−12841.

(22) Neumann, C.; Kaiser, D.; Mohn, M. J.; Füser, M.; Weber, N.-E.; Reimer, O.; Gölzhäuser, A.; Weimann, T.; Terfort, A.; Kaiser, U.; et al. Bottom-Up Synthesis of Graphene Monolayers with Tunable Crystallinity and Porosity. *ACS Nano* **2019**, *13*, 7310−7322.
(23) Matei, D. G.; Weber, N.-E.; Kurasch, S.; Wundrack, S.; Woszczyna, M.; Grothe, M.; Weimann, T.; Ahlers, F.; Stosch, R.; Kaiser, U.; et al. Functional Single-Layer Graphene Sheets from Aromatic Monolayers. *Adv. Mater.* **2013**, *25*, 4146−4151.
(24) Turchanin, A.; Gölzhäuser, A. Carbon Nanomembranes from Self-Assembled Monolayers: Functional Surfaces without Bulk. *Prog. Surf. Sci.* **2012**, *87*, 108−162.
(25) Turchanin, A.; Beyer, A.; Nottbohm, C. T.; Zhang, X.; Stosch, R.; Sologubenko, A.; Mayer, J.; Hinze, P.; Weimann, T.; Gölzhäuser, A. One Nanometer Thin Carbon Nanosheets with Tunable Conductivity and Stiffness. *Adv. Mater.* **2009**, *21*, 1233−1237.
(26) Turchanin, A.; Gölzhäuser, A. Carbon Nanomembranes. *Adv. Mater.* **2016**, *28*, 6075−6103.
(27) Turchanin, A. Synthesis of Molecular 2D Materials via Low-Energy Electron Induced Chemical Reactions. *Chimia* **2019**, *73*, 473−479.
(28) Neumann, C.; Szwed, M.; Frey, M.; Tang, Z.; Kozieł, K.; Cyganik, P.; Turchanin, A. Preparation of Carbon Nanomembranes without Chemically Active Groups. *ACS Appl. Mater. Interfaces* **2019**, *11*, 31176−31181.
(29) Dementyev, P.; Naberezhnyi, D.; Westphal, M.; Buck, M.; Gölzhäuser, A. Carbon Nanomembranes from Aromatic Carboxylate Precursors. *ChemPhysChem* **2020**, *21*, 1006−1011.
(30) Asyuda, A.; de la Morena, R. O.; Sauter, E.; Turner, K.; McDonald, K.; Buck, M.; Zharnikov, M. Electron-Induced Modification of Self-Assembled Monolayers of Aromatic Carboxylic Acids. *J. Phys. Chem. C* **2020**, *124*, 25107−25120.
(31) Krzykawska, A.; Szwed, M.; Ossowski, J.; Cyganik, P. Odd−Even Effect in Molecular Packing of Self-Assembled Monolayers of Biphenyl-Substituted Fatty Acid on Ag(111). *J. Phys. Chem. C* **2018**, *122*, 919−928.
(32) Tao, F.; Bernasek, S. L. Understanding Odd-Even Effects in Organic Self-Assembled Monolayers. *Chem. Rev.* **2007**, *107*, 1408−1453.
(33) Zharnikov, M.; Frey, S.; Rong, H.; Yang, Y.-J.; Heister, K.; Buck, M.; Grunze, M. The Effect of the Sulfur-Metal Bond on the Structure of Self-Assembled Monolayers. *Phys. Chem. Chem. Phys.* **2000**, *2*, 3359−3362.
(34) Rong, H.-T.; Frey, S.; Yang, Y.-J.; Zharnikov, M.; Buck, M.; Wühn, M.; Wöll, C.; Helmchen, G. On the Importance of the Headgroup Substrate Bond in Thiol Monolayers: A Study of Biphenyl-Based Thiols on Gold and Silver. *Langmuir* **2001**, *17*, 1582−1593.
(35) Heister, K.; Rong, H.-T.; Buck, M.; Zharnikov, M.; Grunze, M.; Johansson, L. S. O. Odd-Even Effects at the S-Metal Interface and in the Aromatic Matrix of Biphenyl-Substituted Alkanethiol Self-Assembled Monolayers. *J. Phys. Chem. B* **2001**, *105*, 6888−6894.
(36) Azzam, W.; Cyganik, P.; Witte, G.; Buck, M.; Wöll, C. Pronounced Odd-Even Changes in the Molecular Arrangement and Packing Density of Biphenyl-Substituted Alkanethiol SAMs. *Langmuir* **2003**, *19*, 8262−8270.
(37) Cyganik, P.; Buck, M.; Azzam, W.; Wöll, C. Self-Assembled Monolayers of ω-Biphenyl-Alkane Thiols on Au(111): Influence of Spacer Chain on Molecular Packing. *J. Phys. Chem. B* **2004**, *108*, 4989−4996.
(38) Cyganik, P.; Buck, M. Polymorphism in Biphenyl-Based Self-Assembled Monolayers of Thiols. *J. Am. Chem. Soc.* **2004**, *126*, 5960−5961.
(39) Cyganik, P.; Buck, M.; Strunskus, T.; Shaporenko, A.; Wilton-Ely, J. D. E. T.; Zharnikov, M.; Wöll, C. Competition as a Design Concept: Polymorphism in Self-Assembled Monolayers of Biphenyl-Based Thiols. *J. Am. Chem. Soc.* **2006**, *128*, 13868−13878.
(40) Azzam, W.; Bashir, A.; Terfort, A.; Strunskus, T.; Wöll, C. Combined STM and FTIR Characterization of Terphenylalkanethiol Monolayers on Au(111): Effect of Alkyl Chain Length and Deposition Temperature. *Langmuir* **2006**, *22*, 3647−3655.
(41) Chesneau, F.; Schüpbach, B.; Szelągowska-Kunstman, K.; Ballav, N.; Cyganik, P.; Terfort, A.; Zharnikov, M. Self-Assembled Monolayers of Perfluoroterphenyl-Substituted Alkanethiols: Specific Characteristics and Odd−Even Effects. *Phys. Chem. Chem. Phys.* **2010**, *12*, 12123−12137.
(42) Weidner, T.; Shaporenko, A.; Müller, J.; Schmid, M.; Cyganik, P.; Terfort, A.; Zharnikov, M. The Effect of the Bending Potential on Molecular Arrangement in Alkaneselenolate Self-Assembled Monolayers. *J. Phys. Chem. C* **2008**, *112*, 12495−12506.
(43) Szelagowska-Kunstman, K.; Cyganik, P.; Schüpbach, B.; Terfort, A. Relative Stability of Thiol and Selenol Based SAMs on Au(111)—Exchange Experiments. *Phys. Chem. Chem. Phys.* **2010**, *12*, 4400−4406.
(44) Dendzik, M.; Terfort, A.; Cyganik, P. Odd-even Effect in the Polymorphism of Self-Assembled Monolayers of Biphenyl-Substituted Alkaneselenolates on Au(111). *J. Phys. Chem. C* **2012**, *116*, 19535−19542.
(45) Frey, S.; Rong, H.-T.; Heister, K.; Yang, Y.-J.; Buck, M.; Zharnikov, M. Response of Biphenyl-Substituted Alkanethiol Self-Assembled Monolayers to Electron Irradiation: Damage Suppression and Odd-Even Effects. *Langmuir* **2002**, *18*, 3142−3150.
(46) Vervaecke, F.; Wyczawska, S.; Cyganik, P.; Bastiaansen, J.; Postawa, Z.; Silverans, R. E.; Vandeweert, E.; Lievens, P. Odd-Even Effects in Ion-Beam-Induced Desorption of Biphenyl-Substituted Alkanethiol Self-Assembled Monolayers. *ChemPhysChem* **2011**, *12*, 140−144.
(47) Cisneros, J. A.; Björklund, E.; González-Gil, I.; Hu, Y.; Canales, Á.; Medrano, F. J.; Romero, A.; Ortega-Gutiérrez, S.; Fowler, C. J.; López-Rodríguez, M. L. Structure−Activity Relationship of a New Series of Reversible Dual Monoacylglycerol Lipase/Fatty Acid Amide Hydrolase Inhibitors. *J. Med. Chem.* **2012**, *55*, 824−836.
(48) Citrin, P. H.; Wertheim, G. K.; Baer, Y. Surface-Atom X-ray Photoemission from Clean Metals: Cu, Ag, and Au. *Phys. Rev. B: Condens. Matter Mater. Phys.* **1983**, *27*, 3160−3175.
(49) Krzykawska, A.; Ossowski, J.; Żaba, T.; Cyganik, P. Binding groups for highly ordered SAM formation: carboxylic versus thiol. *Chem. Commun.* **2017**, *53*, 5748−5751.
(50) Heister, K.; Zharnikov, M.; Grunze, M.; Johansson, L. S. O. Adsorption of Alkanethiols and Biphenylthiols on Au and Ag Substrates: A High-Resolution X-ray Photoelectron Spectroscopy Study. *J. Phys. Chem. B* **2001**, *105*, 4058−4061.
(51) Dannenberger, O.; Weiss, K.; Himmel, H.-J.; Jäger, B.; Buck, M.; Wöll, C. An Orientation Analysis of Differently Endgroup-Functionalised Alkanethiols Adsorbed on Au Substrates. *Thin Solid Films* **1997**, *307*, 183−191.
(52) Lamont, C. L. A.; Wilkes, J. Attenuation Length of Electrons in Self-Assembled Monolayers of *n*-Alkanethiols on Gold. *Langmuir* **1999**, *15*, 2037−2042.
(53) Olsen, C.; Rowntree, P. A. Bond-Selective Dissociation of Alkanethiol Based Self-Assembled Monolayers Adsorbed on Gold Substrates, Using Low-Energy Electron Beams. *J. Chem. Phys.* **1998**, *108*, 3750−3764.
(54) Weidner, T.; Ballav, N.; Grunze, M.; Terfort, A.; Zharnikov, M. Modification of Biphenylselenolate Monolayers by Low-Energy Electrons. *Phys. Status Solidi B* **2009**, *246*, 1519−1528.
(55) Yildirim, C.; Füser, M.; Terfort, A.; Zharnikov, M. Modification of Aromatic Self-Assembled Monolayers by Electron Irradiation: Basic Processes and Related Applications. *J. Phys. Chem. C* **2016**, *121*, 567−576.
(56) Taucher, T. C.; Hehn, I.; Hofmann, O. T.; Zharnikov, M.; Zojer, E. Understanding Chemical versus Electrostatic Shifts in X-ray. Photoelectron Spectra of Organic Self-Assembled Monolayers. *J. Phys. Chem. C* **2016**, *120*, 3428−3437.
(57) Otálvaro, D.; Veening, T.; Brocks, G. Self-Assembled Monolayer Induced Au(111) and Ag(111) Reconstructions: Work Functions and Interface Dipole Formation. *J. Phys. Chem. C* **2012**, *116*, 7826−7837.

https://doi.org/10.1021/acs.jpcc.1c01857
J. Phys. Chem. C 2021, 125, 9310−9318

(58) de Boer, B.; Hadipour, A.; Mandoc, M. M.; van Woudenbergh, T.; Blom, P. W. M. Tuning of Metal Work Functions with Self-Assembled Monolayers. *Adv. Mater.* **2005**, *17*, 621−625.
(59) Angelova, P.; Vieker, H.; Weber, N.-E.; Matei, D.; Reimer, O.; Meier, I.; Kurasch, S.; Biskupek, J.; Lorbach, D.; Wunderlich, K.; et al. A Universal Scheme to Convert Aromatic Molecular Monolayers into Functional Carbon Nanomembranes. *ACS Nano* **2013**, *7*, 6489−6497.
(60) Avouris, P.; Persson, B. N. J. Excited States at Metal Surfaces and Their Nonradiative Relaxation. *J. Phys. Chem.* **1984**, *88*, 837−848.

https://doi.org/10.1021/acs.jpcc.1c01857
J. Phys. Chem. C 2021, 125, 9310−9318